Macrophage Sprouty4 deficiency diminishes sepsis-induced acute lung injury in mice

Rong Chen [a,1], Chen Cao [b,1], Huimin Liu [a,1], Wanli Jiang [c], Rui Pan [a], He He [a], Ke Ding [a], Qingtao Meng [a,*]

[a] Department of Anesthesiology, Renmin Hospital of Wuhan University, Wuhan, 430060, China
[b] Medical Center, Renmin Hospital of Wuhan University, Wuhan, 430060, China
[c] Department of Thoracic Surgery, Renmin Hospital of Wuhan University, Wuhan, 430060, China

ARTICLE INFO

ABSTRACT

Objective: Inflammation and oxidative stress play critical roles in sepsis-induced acute lung injury (ALI). Sprout4 (Spry4) is involved in regulating inflammation and tissue injury; however, its role and mechanism in sepsis-induced ALI remain elusive.
Methods: Macrophage-specific Spry4 knockout (Spry4^{MKO}), transgenic (Spry4^{MTG}) mice and matched control littermates were generated and exposed to cecum ligation and puncture (CLP) surgery to establish bacterial sepsis-induced ALI. Bone marrow-derived macrophages (BMDMs) from Spry4^{MKO} or Spry4^{MTG} mice were isolated and subjected to lipopolysaccharide (LPS) stimulation to further validate the role of Spry4 in vitro. To verify the necessity of AMP-activated protein kinase (AMPK), Spry4 and AMPK double knockout mice and compound C were used in vivo and in vitro. BMDMs were treated with STO-609 to inhibit calcium/calmodulin-dependent protein kinase kinase 2 (CaMKK2).
Results: We found that macrophage Spry4 was increased in CLP mice and positively correlated with sepsis-induced ALI. Macrophage Spry4 deficiency prevented, while macrophage Spry4 overexpression exacerbated sepsis-induced inflammation, oxidative stress and ALI in mice and BMDMs. Mechanistic studies revealed that macrophage Spry4 deficiency alleviated sepsis-induced ALI through activating CaMKK2/AMPK pathway.
Conclusion: Our study identify macrophage Spry4 as a promising predictive and therapeutic target of sepsis-induced ALI.

1. Introduction

Sepsis is a devastating clinical disorder, and often causes multiple organ failure among patients in the intensive care unit [1,2]. The lung is one of the most vulnerable organs during sepsis, and septic patients with acute lung injury (ALI) also display higher mortality rates and poorer prognoses, despite the progresses of machine support ventilation and symptomatic treatment [3–5]. It is well-accepted that inflammation and oxidative stress play critical roles in sepsis-induced ALI, and that inhibiting excessive generations of inflammatory cytokines and reactive oxygen species (ROS) significantly improves pulmonary function and survival status [6–8]. AMP-activated protein kinase (AMPK) mainly functions as a central regulator of intracellular energy homeostasis by shifting ATP-consuming anabolism to ATP-producing catabolism;

however, emerging studies have indicating that AMPK extends well beyond its energy-regulating function, and also involves in regulating inflammation and oxidative stress [9–12]. Hu et al. recently demonstrated that activating AMPK could suppress the activations of nuclear factor-κB (NF-κB) and nucleotide-binding oligomerization domain-like receptor with a pyrin domain 3 (NLRP3) inflammasome, thereby reducing inflammation in aging hearts [13]. In addition, results from Yang et al. implied that activating AMPK elevated nuclear factor erythroid 2-related factor 2 (NRF2) protein expression, and subsequently attenuated oxidative damage during lipopolysaccharide (LPS)-induced ALI [14]. Moreover, Jiang et al. also showed that activating AMPK prevented LPS-induced inflammation, oxidative damage and pulmonary dysfunction in mice [15]. These findings identify AMPK as a promising therapeutic target for treating sepsis-induced ALI.

Sprouty (Spry) proteins, consisting of Spry1, Spry2, Spry3 and Spry4, are negative regulators of growth factors-induced receptor tyrosine kinase signaling pathways, and play critical roles in embryonic development and organogenesis [16]. Spry4, a member of Spry proteins, is essential for lung morphogenesis, and Spry4-deficient mice are embryonic lethal and exhibit severe defects in lung morphogenesis [17,18]. In addition, various studies have showing that Spry4 also contributes to inflammation and tissue injury under pathologic stresses. Goldshmit et al. found that inflammation was reduced, while neural function was significantly recovered in Spry4-deficient mice after spinal cord injury [19]. In this study, we used cecum ligation and puncture (CLP) surgery to generate bacterial sepsis-induced ALI in mice, and tried to investigate the role and molecular mechanism of Spry4 during sepsis-induced ALI.

2. Materials and methods

2.1. Reagents

InVivoMab anti-mouse Ly6G (CAT#: BE0075-1) was purchased from Bio X Cell (Lebanon, NH, USA). Compound C (CpC, CAT#: 171260), LPS (*E. coli* O111:B4, CAT#: L4391), STO-609 (STO, CAT#: 570250) and lucigenin (CAT#: M8010) were purchased from Sigma-Aldrich (St. Louis, MO, USA). Mouse interleukin-1β (IL-1β)/IL-1F2 Quantikine ELISA Kit (CAT#: MLB00C) and Mouse IL-6 Quantikine ELISA Kit (CAT#: M6000B) were purchased from R&D Systems, Inc. (Minneapolis, MN, Canada). MojoSort™ Human Pan Monocyte Isolation Kit (CAT#: 480060) was purchased from BioLegend (USA). Human Macrophage Colony-Stimulating Factor (M-CSF) Recombinant Protein (CAT#: RP-8643), Pierce™ BCA Protein Assay Kit (CAT#: 23227) and Amplex Red Hydrogen Peroxide/Peroxidase Assay Kit (CAT#: A22188) were purchased from Invitrogen (Carlsbad, CA, USA). Lactate Dehydrogenase (LDH) Assay Kit (CAT#: A020-2), Myeloperoxidase (MPO) Assay Kit (CAT#: A044-1-1), ROS Assay Kit (CAT#: E004-1-1), Malondialdehyde (MDA) Assay Kit (CAT#: A003-1-1), 4-Hydroxynonenal ELISA Kit (CAT#: H268), Protein Carbonyl Assay Kit (CAT#: A087-1-1), Total Anti-oxidant Capacity Assay Kit (CAT#: A015-2-1) and Superoxide Dismutase (SOD) Assay Kit (CAT#: A001-3-2) were purchased from Nanjing Jiancheng Bioengineering Institute (Nanjing, China). TransAM® NF-κB p65 Kit was purchased from Active Motif (Carlsbad, CA, USA).

2.2. Mice and interventions

Animal experiments were approved by the Ethics Committee of our hospital, and also conformed to the guidelines of the National Institutes of Health. Heterozygous Spry4-floxed (Spry4$^{FL/+}$) mice were generated using CRISPR/Cas9 technology by introducing loxP inserts flanking exon 2 of Spry4 gene. To validate that the two loxP inserts were introduced into the intended sites on the founder mice, two pairs of primers (F1 5′-AAGGGAGTTGTAACTTGTTCACAGC-3′, R1 5′-CTTGA-GAGGCAGGCATTTCTAAATTC-3'; F2 5′-TCTGAGGCGGAAAGAACCAG-3', R2 5′-TTGGGACCAAAGTGTTACTTCTGC-3′) were used. To establish myeloid-specific Spry4 knockout (Spry4^{MKO}) mice, homozygous Spry4$^{FL/FL}$ mice were crossed with LysMcre (The Jackson Laboratory; stock no. 004781) mice on a C57BL6 background. The expression of Cre recombinase may cause additional effects to transgenic mice. Consistent with the instructions in the official website (https://www.jax.org/strain/004781), we also found that homozygous LysMcre mice were viable, fertile, normal in size and did not display any gross physical or behavioral abnormalities. Meanwhile, we also observed no alterations in lung histology and function between LysMcre mice and Spry4$^{FL/FL}$ mice under baseline or after CLP surgery in our preliminary study (data not shown); therefore, we only used Spry4$^{FL/FL}$ mice as the control of Spry4^{MKO} mice. To generate macrophage-specific Spry4 transgenic (Spry4^{MTG}) mice, mouse Spry4 cDNA (NM_011898; CAT#: MC209697, OriGene Technologies, Inc.; Rockville, MD, USA) flanked by the

PiggyBac 5′ and 3′ inverted terminal repeats was subcloned into PiggyBac transposon gene expression donor plasmid containing the CD68 promoter. The PiggyBac donor and helper plasmids were co-injected into zygotes of C57BL/6J mice to obtain Spry4 transgene-positive founder lines. Global AMPKα2 knockout (AKO, stock no. EM: 01419) mice were purchased from the European Mouse Mutant Archive, and backcrossed to the C57BL/6J genetic background for twelve generations. Genotyping of AKO mice was validated using following primers: Primer lox F1 5′-GCTTAGCACGTTACCCTGGATGG-3′, Primer lox R1 5′-GTTATCAGCCCAACTAATTACAC-3′, Primer KOT neoR 5′-GCATT-GAACCACAGTCCTTCCTC-3'. To generate Spry4 and AMPK double knockout (DKO) mice, Spry4^{MKO} mice were crossed with AKO mice. All mice were kept at a SPF barrier system with free access to food and water, and were identified with PCR or western blot before being used.

To establish bacterial sepsis-induced ALI, mice were exposed to CLP surgery as previously described [20]. Briefly, 8- to 12-week-old male mice were anesthetized with ketamine (80–100 mg/kg, i.p.) and xylazine (10 mg/kg, i.p.), and then subjected to an abdominal incision with the cecum exposed. Next, the cecum was ligated with 3-0 silk at 75% of the distance between distal pole and the base, and punctured twice using a 21-gauge needle close to the distal end. A small amount of feces was extruded. Then, the cecum was repositioned and the abdomen was closed in two layers with 5-0 suture. After surgery, mice were subcutaneously injected with 1 mL pre-warmed sterile saline for liquid resuscitation, and placed at 37 °C to keep warm. Ibuprofen (250 μg/mL in drinking water) was used for pre- and post-operative analgesia. Sham-operated mice underwent the same surgical procedure but not ligation and puncture. For chimeras studies, recipient mice were irradiated twice by lethal X-ray irradiation (6.5 Gy), and then 5×10^6 bone marrow cells isolated from the tibia and femurs of donor mice were injected into recipients through the tail vein [21,22]. Peripheral blood from the chimera mice was used for PCR analysis of hematologic chimerism. Four weeks after bone marrow transplantation, mice were exposed to CLP surgery. Twenty-four hours after CLP surgery, mice were sacrificed for molecular and histological analysis. Survival rate was monitored every 12 h. To deplete neutrophils, mice were injected with Ly6G antibody (500 μg per mouse, i.p.) 24 h and 2 h before CLP surgery, while control mice were treated with isotypic IgG [22]. To inhibit AMPK in vivo, mice were injected with CpC (20 mg/kg, i.p.) once two days from 1 week before CLP surgery [15].

2.3. Histological analysis

Lungs were excised and immersed in 4% formaldehyde solution for 48 h, which were then embedded with paraffin and sliced into 3 μm thick sections. Next, lung slices were subjected to Hematoxylin-Eosin staining, and the inflammation score was independently measured by three pathologists blinded to the groups as previously described [6].

2.4. Bronchoalveolar lavage fluid (BALF) analysis

To obtain BALF, lungs were intratracheally lavaged with 1 mL pre-cold sterile phosphate buffer saline (PBS) for 3 times, and then the liquid was centrifuged for 5 min at 4 °C at 1500 rpm. The sedimented cell pellets were re-suspended with 0.5 mL PBS and counted with a hemocytometer and Wright-Giemsa staining. Cell-free supernatants were subjected to ELISA analysis of inflammatory cytokines.

2.5. Lung wet to dry ratio

Lung wet to dry ratio was calculated to evaluate pulmonary edema as previously described [8,15]. Briefly, fresh lungs were excised and weighed to obtain the wet weight after removing the blood, which were then placed in an 80 °C oven to obtain the constant dry weight.

2.6. Pulmonary function measurement

Pulmonary function was measured using the Buxco pulmonary function testing system (Sharon, Connecticut, CT, USA), and airway resistance, lung compliance and pulmonary ventilation were calculated as previously described [6].

2.7. Arterial blood gas measurement

Arterial blood was collected from the descending aorta and subjected to blood gas measurement to evaluate pulmonary gas exchange and blood acid-base status. Partial pressure of oxygen (PaO_2), partial pressure of carbon dioxide ($PaCO_2$) and calculated total carbon dioxide (TCO_2) were measured using an automatic blood gas analyzer as previously described [23].

2.8. Microarray analysis

Three gene expression profiles (GSE15379, GSE40180 and GSE165226) were downloaded from GEO database, and all these data were generated from lung samples of CLP-operated septic mice or Sham-operated control mice. Microarray data were integrated and data processing were performed using R software with the limma package. Differentially expressed genes (DEGs) were defined as |$\log_2$ (Fold Change)|>1 and a P value < 0.05, which were then intersected to obtain the overlapped DEGs.

2.9. Cell isolation and culture

To isolate bone marrow-derived macrophages (BMDMs), the tibia and femurs were collected from 6- to 8-week-old male mice, whose bone marrows were extracted. These bone marrow cells were cultured in DMEM containing 10% fetal bovine serum (FBS) and 30% L929 conditioned medium for 7 days to induce differentiation of BMDMs [21,22]. Peripheral blood mononuclear cells (PBMCs) were isolated from blood samples of septic patients with or without ALI and control patients using the MojoSort™ Human Pan Monocyte Isolation Kit following the manufacturer's instructions. To induce differentiation of human monocyte-derived macrophages (HMDMs), human PBMCs from control patients were cultured with RPMI 1640 containing 10% FBS and 100 ng/mL M-CSF for 6 days [21]. BALF was collected and centrifuged to obtain the cells, which were then re-suspended with DMEM containing 10% FBS and allowed to adhere for 1 h to obtain the alveolar macrophages (AMs) [24]. In the in vitro studies, macrophages were stimulated with LPS (100 ng/mL) for 12 h [8,15]. For AMPK inhibition, macrophages from Spry4^FL/FL or Spry4^MKO mice were pre-treated with CpC (20 μmol/L) for 24 h before LPS stimulation [15]. For calcium/calmodulin-dependent protein kinase kinase 2 (CaMKK2) inhibition, macrophages were treated with STO (5 mmol/L) together with LPS stimulation [25].

2.10. Western blot

Lung or cell samples were lysed in RIPA buffer and quantified using a Pierce™ BCA Protein Assay Kit according to the manufacturer's instructions. Next, protein lysates were subjected to 10% sodium dodecyl sulfate-polyacrylamide gel electrophoresis and transferred onto polyvinylidene fluoride membranes [26–28]. Primary antibodies were as following: *anti*-Spry4 (CAT#: ab7513, Abcam), anti-glyceraldehyde-3-phosphate dehydrogenase (GAPDH, CAT#: ab8245, Abcam), *anti*-NRF2 (CAT#: ab62352, Abcam), *anti*-phospho AMPK (p-AMPK, CAT#: 2535, CST), anti-total AMPK (t-AMPK, CAT#: 2532, CST), *anti*-p-CaMKK2 (CAT#: 16737, CST), *anti-t*-CaMKK2 (CAT#: 16810, CST). After visualized with horseradish peroxidase (HRP)-conjugated secondary antibodies and Ultra High Sensitivity ECL Substrates (CAT#: ab133409, Abcam), the blots were scanned by a gel imaging system, and analyzed using the Image Lab software (Bio-Rad, Hercules, CA, USA).

2.11. Quantitative real-time PCR

Total RNA was extracted using RNeasy Mini Kit (Cat#: 74104, Qiagen) following standard protocols, and reverse transcription was performed using GoScript™ Reverse Transcription System (Cat#: A5000, Promega). Quantitative real-time PCR was performed using SYBR GreenER™ qPCR SuperMix Universal (Cat#: 1176202K, Invitrogen), and gene expression was calculated using the $2^{-\Delta\Delta CT}$ method with GAPDH as the internal control [29–32]. The primer sequences were listed as following: mouse Spry1 forward: 5′-GGTCATAGGTCA GATCGGGTC-3′, reverse 5′-CTTGCCACACTGTTCGCAG-3′; mouse Spry2 forward: 5′-TCCAAGAGATGCCCTTACCCA-3′, reverse 5′-GCA-GACCGTGGAGTCTTTCA-3'; mouse Spry3 forward: 5′-GTAAACAAGCT CTTTCTAGCCCT-3′, reverse 5′-AGTGGTGCTTTGGGACATTGA-3′; mouse Spry4 forward: 5′-GCAGCGTCCCTGTGAATCC-3′, reverse 5′-TCTGGTCAATGGGTAAGATGGT-3′; human Spry4 forward: 5′-TCTG ACCAACGGCTCTTAGAC-3′, reverse 5′-GTGCCATAGTTGACCAGA GTC-3'.

2.12. Measurements of LDH, MPO and NF-κB activities

LDH activity in fresh lung samples was detected using an LDH Assay Kit according to the manufacturer's instructions, and the absorbance was measured at 450 nm with a Multiskan Spectrum Microplate Reader (Thermo, Waltham, MA, USA) [33]. To measure MPO activity, fresh lung homogenates were prepared and reacted with relevant reagents according to the manufacturer's instructions of a commercial kit. To measure NF-κB transcription activity, fresh nuclear proteins were prepared from lung samples, and added to oligonucleotide-coated plates. Next, the transcription factors were incubated with NF-κB primary antibodies and HRP-conjugated secondary antibodies. Finally, the absorbance was measured on a spectrophotometer at 450 nm with an optional reference wavelength of 655 nm.

2.13. Measurements of oxidative stress

To measure ROS in vivo and in vitro, fresh lung homogenates and cell lysates were incubated with 2′,7′-Dichlorofluorescin Diacetate (DCFH-DA, 50 μmol/L) for 30 min, and DCF intensity was measured using a spectrofluorometer with an excitation wavelength of 502 nm and emission at 530 nm [34,35]. To measure hydrogen peroxide (H_2O_2), fresh lung tissue blocks (10–20 mg) or cells were incubated with Amplex Red (100 μmol/L) and horseradish peroxidase (1 U/mL) for 30 min at 37 °C in the dark, and then the supernatant was collected and transferred to 96-well plates with the absorbance measured at 560 nm [36]. Superoxide (O_2^-) production was measured using a lucigenin chemiluminescence assay [36]. Briefly, fresh lung homogenates or cell lysates were incubated with 5 μmol/L lucigenin and 500 μmol/L NADH or NADPH for 10 min at 37 °C in the dark. The chemiluminescence was measured by an AB-2200 Luminescence PSN luminometer (ATTO, Nagoya, Japan) at 1 min intervals over a 5 min period. To measure lipid and protein peroxidation, fresh lung samples were homogenized and used to detecting productions of MDA, 4-HNE, protein carbonyl, TAOC and total SOD activity according to the manufacturer's instructions [37, 38].

2.14. RNA-seq and data analysis

Total RNA was extracted from lungs of Spry4^FL/FL or Spry4^MKO mice with CLP surgery, and reversely transcribed into double strand cDNA fragments. The RNA quality and integrity were evaluated using the Agilent Technologies 2100 Bioanalyzer. RNA-seq library was generated using Dynabeads mRNA DIRECT Micro Purification Kit (Thermo Fisher

Scientific) and ScriptSeq v2 RNA-Seq Library Preparation Kit (Epicentre) according to the manufacturer's instructions, which was then sequenced on Illumina HiSeq2500 using TruSeq SBS Kit v3-HS. After adaptor-removing and quality control filtering, the high-quality clean reads were mapped to mouse genome (mm10) using HISAT2. DEGs were defined as $|\log_2 (Fold\ Change)|>1$ and an adj P value < 0.05. Heat maps were used to evaluate DEGs, while Kyoto Encyclopedia of Genes and Genomes (KEGG) pathway analysis was performed to determine the significant functions and pathways of DEGs.

2.15. Patients and clinical samples

Blood samples of septic or control patients were obtained from our hospital, and the experimental procedures were approved by the Medical Research Ethics Committee. Written informed consent was obtained from all subjects, and all experiments were conducted in accordance with the principles of the Declaration of Helsinki.

2.16. Statistical analysis

Data are expressed as the mean $\pm$ standard deviation (SD) and statistical analysis was performed using SPSS 23.0 software. A two-tailed unpaired Student's t-test and a one-way analysis of variance (ANOVA), followed by Tukey's post hoc comparisons test were performed to compare differences between 2 groups or among multiple groups, respectively. Pearson correlation coefficient test was used to detect correlation between Spry4 expression and pulmonary injury. Differences with P values < 0.05 were considered statistically significant.

3. Results

3.1. Macrophage Spry4 is increased in CLP mice and positively correlates with sepsis-induced ALI

To mine the pivotal genes altered during sepsis-induced ALI, we intersected three gene expression profiles (GSE15379, GSE40180 and GSE165226) to obtain the overlapped DEGs from CLP-injured mouse lungs. As shown in Fig. 1A and supplementary Table, 45 DEGs were identified. Among these DEGs, we focused on Spry4, a negative regulator of growth factors-induced receptor tyrosine kinase signaling pathways. As shown in Fig. 1B, Spry4 expressed was increased in all three gene expression profiles. Accordingly, we also found that Spry4 protein was significantly elevated in lungs and AMs of CLP mice (Fig. 1C). In addition, Spry4 expression in AMs positively correlated with pulmonary LDH activity, an index of pulmonary injury (Fig. 1D). To measure Spry4 expression in macrophages in vitro, BMDMs and HMDMs were treated with LPS. As shown in Fig. 1E and F, macrophage Spry4 mRNA was increased in LPS-stimulated BMDMs and HMDMs. To confirm Spry4 upregulation, we also determined Spry4 mRNA in circulating PBMCs from septic patients. Interestingly, Spry4 mRNA was also increased in PBMCs from septic patients (Fig. 1G). Moreover, septic patients with ALI exhibited higher Spry4 expression in PBMCs than those without ALI (Fig. 1H). To clarify the diagnostic role of Spry4 expression in PBMCs on septic ALI, we divided septic patients into low-Spry4 and high-Spry4 groups using the median Spry4 mRNA in PBMCs as the threshold. Compared with the low-Spry4 group, patients with higher Spry4 in PBMCs exhibited worse pulmonary function, as evidenced by decreased PaO_2 and increased $PaCO_2$ (Fig. 1I). These findings indicate that macrophage Spry4 is increased in CLP mice and positively correlates with sepsis-induced ALI.
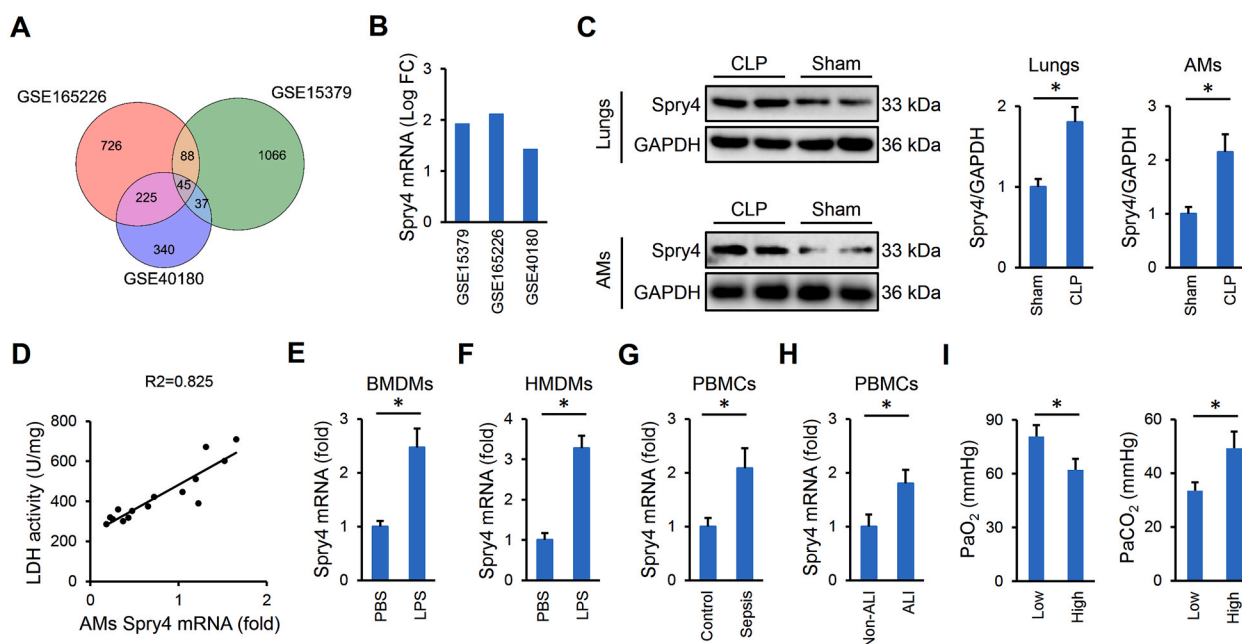

Fig. 1. Macrophage Spry4 is increased in CLP mice and positively correlates with sepsis-induced ALI. (A) Identification of 45 DEGs from the three gene expression profiles. (B) Relative Spry4 expression in CLP-injured lungs from the three gene expression profiles. (C) Mice were exposed to CLP surgery for 24 h, and then fresh lungs and AMs were prepared to detect Spry4 expression using western blot (n = 6). (D) Spry4 mRNA expression in AMs positively correlated with LDH activity in lungs (n = 15). (E-F) BMDMs and HMDMs were stimulated with LPS (100 ng/mL) for 12 h, and then Spry4 mRNA was detected using quantitative real-time PCR (n = 6). (G) PBMCs were isolated from septic or control patients, and Spry4 mRNA was detected (n = 6). (H) PBMCs were isolated from septic patients with or without ALI, and Spry4 mRNA was detected (n = 6). (I) Septic patients were divided into low-Spry4 and high-Spry4 groups using the median Spry4 mRNA in PBMCs as the threshold, and then gas exchange function was evaluated by PaO_2 and $PaCO_2$ (n = 6). Data are expressed as the mean $\pm$ SD. $*P < 0.05$.

3.2. Macrophage Spry4 deficiency prevents sepsis-induced ALI in mice

To better clarify the role of macrophage Spry4 in regulating sepsis-induced ALI, we used the Cre-LoxP system to create Spry4^MKO mice. As shown in Fig. 2A and B, Spry4 mRNA and protein levels were significantly reduced in macrophages from Spry4^MKO mice, compared with those from Spry4^FL/FL mice, while no alterations of Spry1, Spry2 or Spry3 mRNA in macrophages were observed between groups. Results from Hematoxylin-Eosin staining indicated that macrophage Spry4 deficiency obviously attenuated CLP-induced ALI, as evidenced by improved pulmonary congestion, thickening of the alveolar wall and inflammatory infiltration (Fig. 2C and D). And increased LDH activity, an index for cellular damage, was also decreased in macrophage Spry4-deficient mice upon CLP surgery (Fig. 2E). Furthermore, macrophage Spry4 deficiency also remarkably decreased lung wet to dry ratio and total proteins in BALF, indicating decreased pulmonary edema and injury (Fig. 2F and G). Accordingly, respiratory dysfunction of CLP mice, as evidenced by increased airway resistance, decreased lung compliance and pulmonary ventilation, was attenuated in mice with macrophage Spry4 deficiency (Fig. 2H–J). Results from arterial blood gas analysis implied that macrophage Spry4 deficiency significantly alleviated gas exchange impairment of CLP mice, as evidenced by increased PaO$_2$ and decreased PaCO$_2$, TCO$_2$ (Fig. 2K-M). More importantly, Spry4^MKO mice exhibited lower mortality rate than Spry4^FL/FL mice upon CLP surgery (Fig. 2N). Collectively, these data imply that macrophage Spry4 deficiency prevents sepsis-induced ALI in mice.

3.3. Macrophage Spry4 deficiency reduces sepsis-induced pulmonary inflammation and oxidative stress

Inflammation and oxidative stress play critical roles in the

progression of sepsis-induced ALI. As expected, CLP surgery significantly elevated IL-1β and IL-6 in BALF, which were remarkably reduced by macrophage Spry4 deficiency (Fig. 3A). In addition, macrophage Spry4 deficiency also suppressed CLP-induced accumulations of total cells, macrophages and neutrophils in BALF (Fig. 3B). And CLP-induced elevation of MPO activity, an index of neutrophil accumulation in lungs, was also suppressed in Spry4^MKO mice than that in Spry4^FL/FL mice (Fig. 3C). NF-κB functions as a pivotal transcription factor to trigger the expression of various inflammatory cytokines, including IL-1β and IL-6. Interestingly, macrophage Spry4 deficiency significantly inhibited NF-κB transcription activity in CLP-injured lungs (Fig. 3D). Meanwhile, CLP-induced overproductions of free radicals were also decreased by macrophage Spry4 deficiency, as evidenced by decreased levels of DCF intensity, H$_2$O$_2$ and O$_2^-$ (Fig. 3E and F). And Spry4^MKO mice also exhibited lower levels of MDA, 4-HNE and protein carbonyls than Spry4^FL/FL mice after CLP surgery, indicating improved lipid and protein peroxidation (Fig. 3G and H). NRF2 is a key transcription factor in regulating redox homeostasis through triggering the expression of various anti-oxidant enzymes. As shown in Fig. 3I, NRF2 expression was significantly decreased in CLP-injured lungs, which was prevented by macrophage Spry4 deficiency. Accordingly, CLP-induced suppressions on TAOC and total SOD activity were dramatically restored in macrophage Spry4-deficient mice (Fig. 3J and K).

Next, we performed bone marrow transplantation to confirm the effects of macrophage Spry4 in CLP-induced ALI. Spry4^FL/FL mice were lethally irradiated and reconstituted with bone marrow from either Spry4^FL/FL mice or Spry4^MKO mice. As shown in Figure S1A-B, CLP-induced inflammation in lungs was alleviated in Spry4^FL/FL mice receiving Spry4^MKO bone marrows, as evidenced by decreased IL-1β and IL-6 in BALF, and decreased MPO activity in lungs. In addition, Spry4^MKO→Spry4^FL/FL chimeras exhibited fewer generations of free
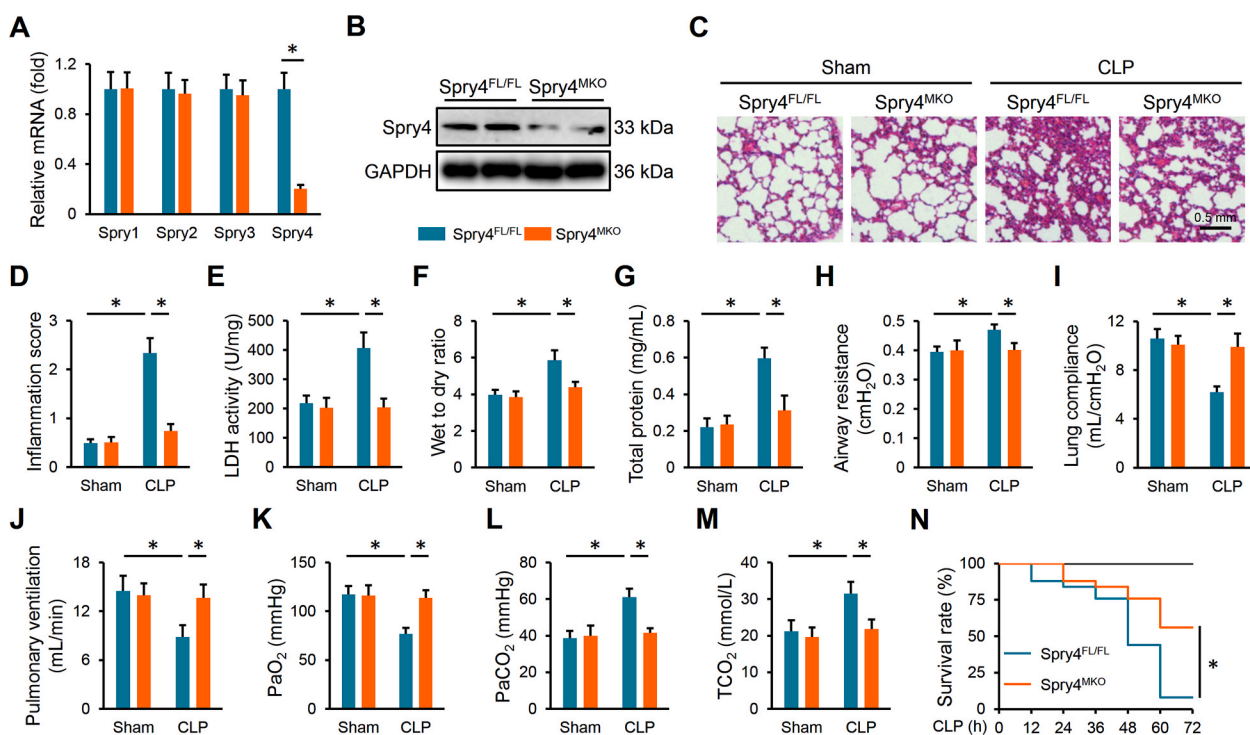

Fig. 2. Macrophage Spry4 deficiency prevents sepsis-induced ALI in mice. (A) BMDMs were isolated from Spry4^FL/FL mice and Spry4^MKO mice, and levels of Spry1, Spry2, Spry3 and Spry4 in BMDMs were detected using quantitative real-time PCR (n = 6). (B) BMDMs were isolated from Spry4^FL/FL mice and Spry4^MKO mice, and Spry4 protein level was measured using western blot (n = 6). (C) Spry4^FL/FL mice and Spry4^MKO mice were subjected to CLP surgery for 24 h, and mouse lungs were excised and subjected to Hematoxylin-Eosin staining (n = 6). (D) Inflammation score of Hematoxylin-Eosin staining (n = 6). (E) LDH activity in fresh lungs (n = 6). (F) Lung wet to dry ratio (n = 6). (G) Total proteins in BALF (n = 6). (H–J) Pulmonary function as assessed by airway resistance, lung compliance and pulmonary ventilation (n = 6). (K–M) Arterial blood gas analysis of PaO$_2$, PaCO$_2$ and TCO$_2$ (n = 6). (N) Survival rate in Spry4^FL/FL mice and Spry4^MKO mice after CLP surgery. Data are expressed as the mean ± SD. *P < 0.05.
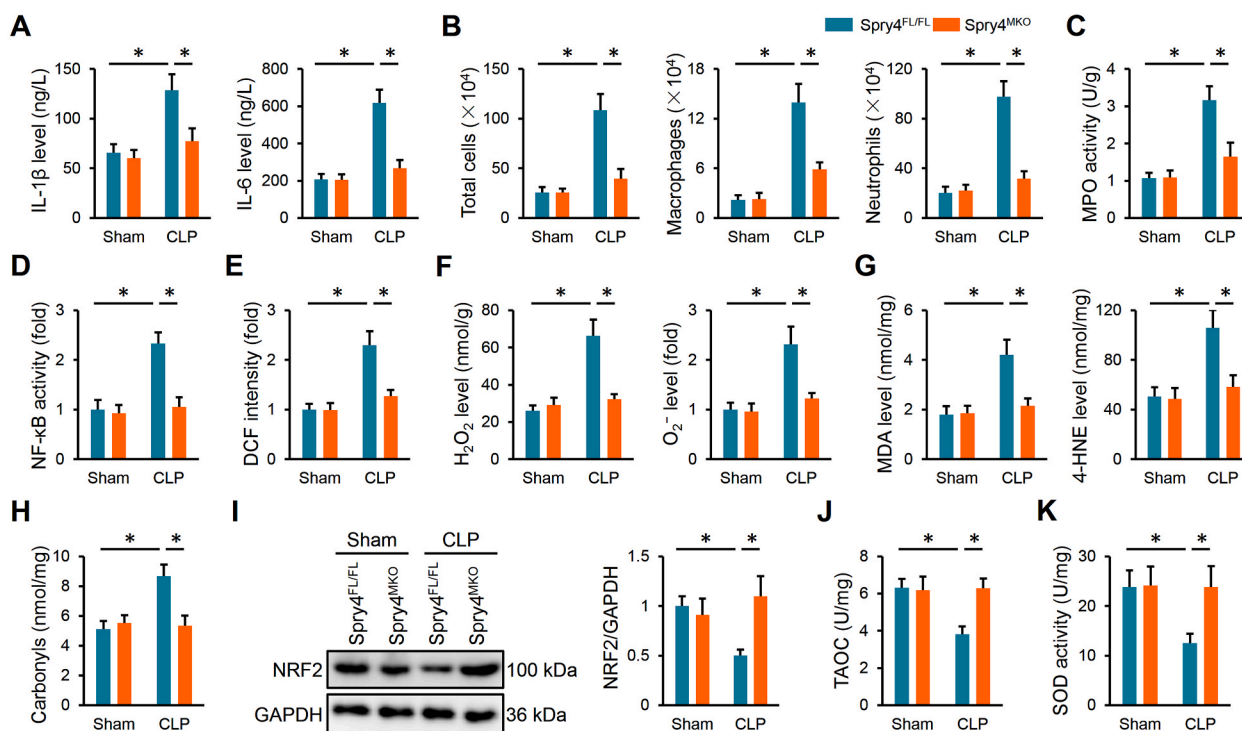
Fig. 3. Macrophage Spry4 deficiency reduces sepsis-induced pulmonary inflammation and oxidative stress. (A) Spry4$^{FL/FL}$ mice and Spry4^{MKO} mice were subjected to CLP surgery for 24 h, and BALF was collected for the analysis of IL-1β and IL-6 (n = 6). (B) Numbers of total cells, macrophages and neutrophils were determined in BALF (n = 6). (C) MPO activity in lungs (n = 6). (D) NF-κB activity in lungs (n = 6). (E) Relative ROS level in lungs as assessed by DCF intensity (n = 6). (F) Quantification of H_2O_2 and O_2^- in lungs (n = 6). (G-H) Quantification of MDA, 4-HNE and protein carbonyls in lungs (n = 6). (I) NRF2 protein level in lungs (n = 6). (J-K) Quantification of TAOC and total SOD activity in lungs (n = 6). Data are expressed as the mean $\pm$ SD. *$P < 0.05$.
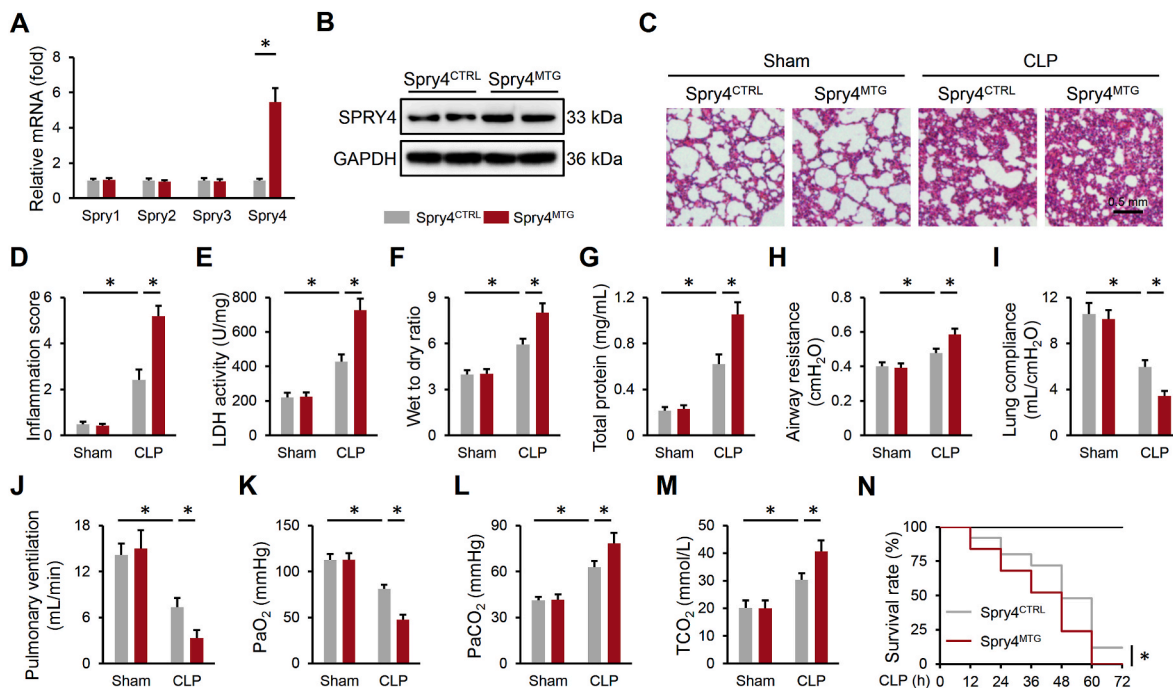

Fig. 4. Macrophage Spry4 overexpression exacerbates sepsis-induced ALI in mice. (A) BMDMs were isolated from Spry4^{CTRL} mice and Spry4^{MTG} mice, and levels of Spry1, Spry2, Spry3 and Spry4 in BMDMs were detected using quantitative real-time PCR (n = 6). (B) BMDMs were isolated from Spry4^{CTRL} mice and Spry4^{MTG} mice, and Spry4 protein level was measured using western blot (n = 6). (C) Spry4^{CTRL} mice and Spry4^{MTG} mice were subjected to CLP surgery for 24 h, and mouse lungs were excised and subjected to Hematoxylin-Eosin staining (n = 6). (D) Inflammation score of Hematoxylin-Eosin staining (n = 6). (E) LDH activity in fresh lungs (n = 6). (F) Lung wet to dry ratio (n = 6). (G) Total proteins in BALF (n = 6). (H–J) Pulmonary function as assessed by airway resistance, lung compliance and pulmonary ventilation (n = 6). (K–M) Arterial blood gas analysis of PaO$_2$, PaCO$_2$ and TCO$_2$ (n = 6). (N) Survival rate in Spry4^{CTRL} mice and Spry4^{MTG} mice after CLP surgery. Data are expressed as the mean $\pm$ SD. *$P < 0.05$.

radicals in lungs from CLP mice (Figure S1C-D). Consistent with the molecular alterations, Spry4$^{FL/FL}$ mice reconstituted with Spry4^{MKO} bone marrows exhibited mild pulmonary injury, edema and dysfunction upon CLP surgery, as evidenced by decreased inflammation score, LDH activity, lung wet to dry ratio, PaCO$_2$ and TCO$_2$, and increased PaO$_2$ (Figure S1E-H). To further exclude the effect of Spry4 in polymorphonuclear neutrophils during sepsis-induced ALI, we also depleted neutrophils using *anti*-Ly6G. As shown in Figure S2A-H, Spry4^{MKO} mice suffered less CLP-induced ALI than Spry4$^{FL/FL}$ mice, regardless of *anti*-Ly6G antibody treatment, eliminating the involvement of neutrophils in this process. These findings suppose that macrophage Spry4 deficiency reduces sepsis-induced pulmonary inflammation and oxidative stress.

3.4. Macrophage Spry4 overexpression exacerbates sepsis-induced ALI in mice

To further verify the role of macrophage Spry4 in sepsis-induced ALI, we generated Spry4^{MTG} mice. As shown in Fig. 4A and B, it was Spry4, instead of other Spry proteins, was significantly elevated in macrophages from Spry4^{MTG} mice. CLP-induced pulmonary injury and edema were significantly aggravated in Spry4^{MTG} mice, as evidenced by increased inflammation score, LDH activity, lung wet to dry ratio and total proteins in BALF (Fig. 4C-G). Accordingly, CLP-induced elevation of airway resistance, and suppression of lung compliance and pulmonary ventilation were further compromised in mice with macrophage Spry4 overexpression (Fig. 4H-J). Meanwhile, macrophage Spry4 overexpression also exacerbated gas exchange impairment and mortality rate of CLP mice (Fig. 4K-N). Taken together, we demonstrate that macrophage Spry4 overexpression exacerbates sepsis-induced ALI in mice.

3.5. Macrophage Spry4 overexpression facilitates sepsis-induced pulmonary inflammation and oxidative stress

In line with the phenotypic alteration, Spry4^{MTG} mice also exhibited higher IL-1β and IL-6 in BALF than control Spry4^{CTRL} mice after CLP surgery (Fig. 5A). And CLP-induced accumulations of total cells, macrophages and neutrophils in BALF were also aggravated by macrophage Spry4 overexpression (Fig. 5B and C). In addition, macrophage Spry4 overexpression further elevated NF-κB transcription activity in CLP-injured lungs (Fig. 5D). Meanwhile, CLP-induced oxidative stress was further amplified in lungs of Spry4^{MTG} mice, as evidenced by increased levels of DCF intensity, H$_2$O$_2$, O$_2^-$, MDA, 4-HNE and protein carbonyls (Fig. 5E-H). In contrast, NRF2 expression, and downstream TAOC as well as total SOD activity in lungs were further inhibited by macrophage Spry4 overexpression after CLP surgery (Fig. 5I-K). In general, we reveal that macrophage Spry4 overexpression facilitates sepsis-induced pulmonary inflammation and oxidative stress.

3.6. Spry4 deficiency attenuates, while Spry4 overexpression promotes LPS-induced inflammation and oxidative stress in BMDMs

We also stimulated BMDMs from Spry4^{MKO} mice or Spry4^{MTG} mice with LPC to further validate the role of macrophage Spry4 in vitro. As shown in Figure S3A, BMDMs from Spry4^{MKO} mice exhibited lower levels of IL-1β and IL-6 in the medium after LPS stimulation. LPS-induced increases of DCF intensity, H$_2$O$_2$ and O$_2^-$ were also reduced in BMDMs from Spry4^{MKO} mice (Figure S3B). And Spry4 deficiency significantly restored TAOC and total SOD activity in LPS-stimulated BMDMs (Figure S3C). In contrast, BMDMs from Spry4^{MTG} mice exhibited higher levels of IL-1β, IL-6, DCF intensity, H$_2$O$_2$ and O$_2^-$, indicating an exacerbated inflammation and oxidative stress (Figure S3D-F). Meanwhile, TAOC and total SOD activity in BMDMs from Spry4^{MTG} mice were further decreased after LPS stimulation (Figure S3G). Together, our
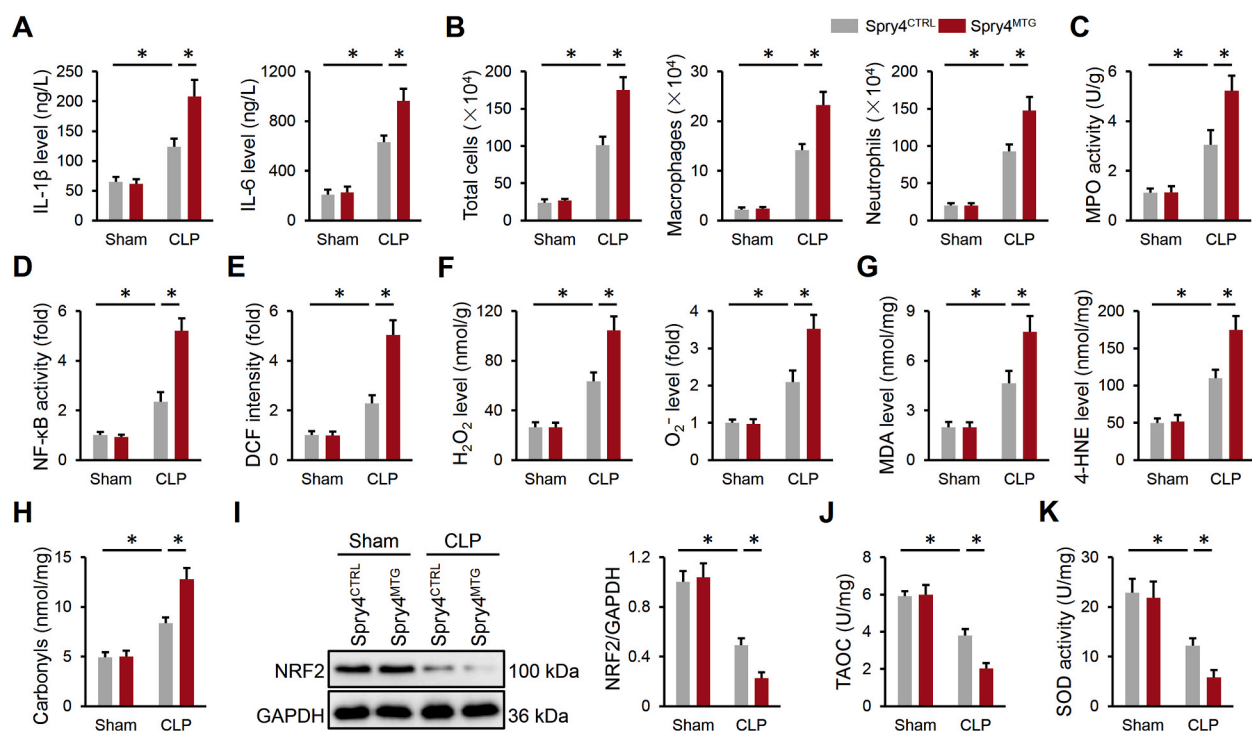

Fig. 5. Macrophage Spry4 overexpression facilitates sepsis-induced pulmonary inflammation and oxidative stress. (A) Spry4^{CTRL} mice and Spry4^{MTG} mice were subjected to CLP surgery for 24 h, and BALF was collected for the analysis of IL-1β and IL-6 (n = 6). (B) Numbers of total cells, macrophages and neutrophils were determined in BALF (n = 6). (C) MPO activity in lungs (n = 6). (D) NF-κB activity in lungs (n = 6). (E) Relative ROS level in lungs as assessed by DCF intensity (n = 6). (F) Quantification of H$_2$O$_2$ and O$_2^-$ in lungs (n = 6). (G-H) Quantification of MDA, 4-HNE and protein carbonyls in lungs (n = 6). (I) NRF2 protein level in lungs (n = 6). (J-K) Quantification of TAOC and total SOD activity in lungs (n = 6). Data are expressed as the mean ± SD. *P < 0.05.

data reveal that Spry4 deficiency attenuates, while Spry4 over-expression promotes LPS-induced inflammation and oxidative stress in BMDMs.

3.7. Macrophage Spry4 deficiency alleviates sepsis-induced ALI through activating AMPK pathway

To further clarify the role of macrophage Spry4 in sepsis-induced ALI, we performed gene profiling of CLP-injured lungs from Spry4[MKO] mice and Spry4[FL/FL] mice. In line with above-mentioned results, expressions of inflammatory genes were decreased, while expressions of anti-oxidant genes were increased in lungs from Spry4[MKO] mice after CLP surgery (Fig. 6A). KEGG pathway analysis of DEGs revealed that AMPK pathway showed the highest correlation with macrophage Spry4 deficiency in CLP-injured lungs (Fig. 6B). Consistently, we also found that macrophage Spry4 deficiency activated, while macrophage Spry4 overexpression inhibited AMPK pathway in CLP-injured lungs (Fig. 6C–E). To further validate the necessity of AMPK, we crossed Spry4[MKO] mice with AKO mice to establish DKO mice (Figure S4). As shown in Fig. 6F–H, AMPK deletion significantly blocked the anti-inflammatory and anti-oxidant effects in Spry4[MKO] mice after CLP surgery, as evidenced by increased IL-1β, IL-6, H_2O_2, O_2^- and DCF intensity. Consistently, macrophage Spry4 deficiency-mediated inhibitory effects on inflammation score, LDH activity, pulmonary edema and gas exchange impairment were also blunted in DKO mice (Fig. 6I-L). In addition, we also used CpC, a pharmacological inhibitor of AMPK activity, to further verify the involvement of AMPK pathway in vivo and in

vitro. As shown in Figure S5A-C, CpC treatment significantly blocked macrophage Spry4 deficiency-mediated anti-inflammatory and anti-oxidant effects in CLP-injured lungs. And the protective effects against CLP-induced pulmonary injury, edema and gas exchange impairment were also blunted in CpC-treated mice, as evidenced by increased inflammation score, LDH activity, lung wet to dry ratio, $PaCO_2$, and decreased PaO_2 (Figure S5D-G). In line with the in vivo findings, we also found that CpC treatment significantly blocked the inhibitory effects against LPS-induced inflammation and oxidative stress in Spry4[MKO] BMDMs (Figure S6A-C). Collectively, we prove that macrophage Spry4 deficiency alleviates sepsis-induced ALI through activating AMPK pathway.

3.8. Macrophage Spry4 deficiency activates AMPK pathway through CaMKK2

Subsequently, we determined the possible mechanism mediating AMPK activation by macrophage Spry4 deficiency. It is well-accepted that CaMKK2 and liver kinase B1 are two primary upstream kinases activating AMPK pathway [25]. As shown in Fig. 6B, calcium signaling pathway was significantly altered by macrophage Spry4 deficiency during CLP-induced ALI, and CaMKK2 is a calcium-dependent kinase. Therefore, we investigated whether macrophage Spry4 deficiency activates AMPK pathway through CaMKK2. As shown in Fig. 7A, CaMKK2 was activated in CLP-injured lungs from Spry4[MKO] mice. To verify the necessity of CaMKK2, we treated BMDMs with STO to inhibit CaMKK2. As expected, STO treatment blocked AMPK activation in Spry4[MKO]
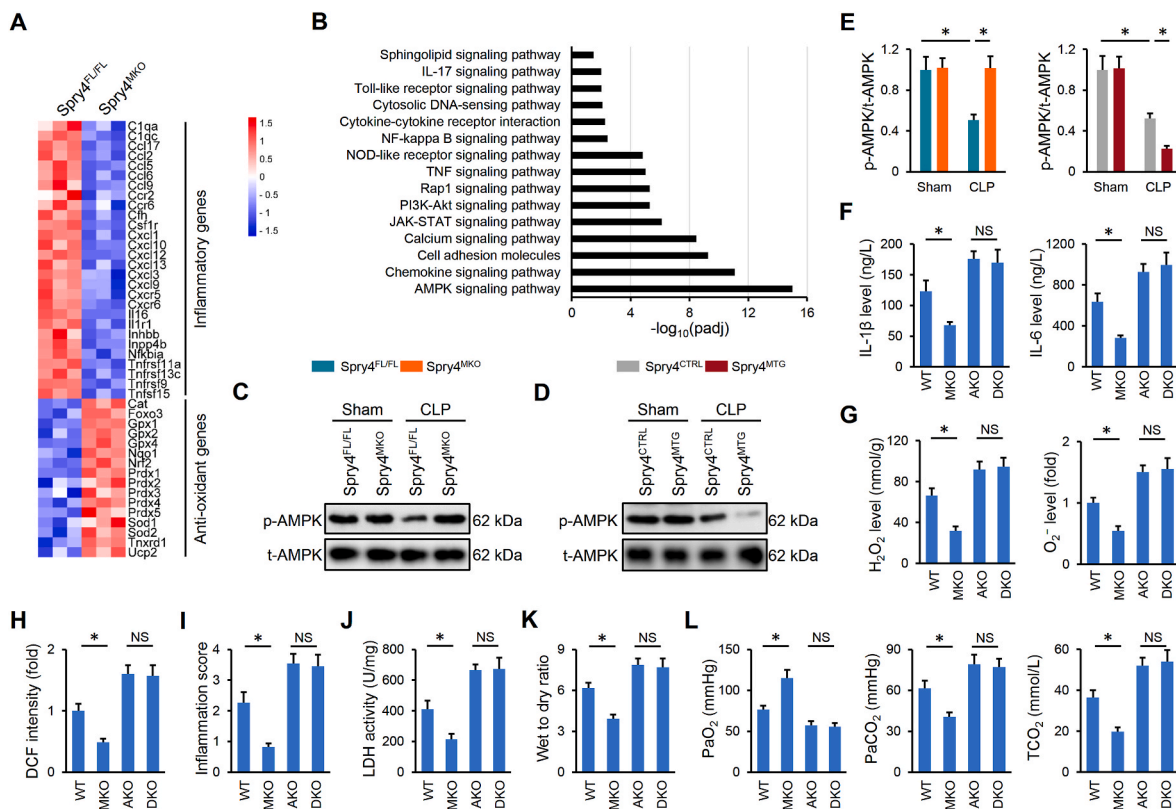

Fig. 6. Macrophage Spry4 deficiency alleviates sepsis-induced ALI through activating AMPK pathway. (A) Heat maps showing the expression profile of genes related to inflammatory and anti-oxidant events in CLP-injured lungs from Spry4[FL/FL] mice and Spry4[MKO] mice based on RNA-seq analysis (n = 3). (B) Top 15 KEGG pathways altered in CLP-injured lungs from Spry4[FL/FL] mice and Spry4[MKO] mice (n = 3). (C–E) Spry4[MKO] mice, Spry4[MTG] mice and matched control littermates were subjected to CLP surgery for 24 h, and AMPK phosphorylation was detected using western blot (n = 6). (F) Spry4[MKO] mice, AKO mice, Spry4 and AMPK DKO mice and wild type (WT) mice were subjected to CLP surgery for 24 h, and BALF was collected for the analysis of IL-1β and IL-6 (n = 6). (G) Quantification of H_2O_2 and O_2^- in lungs (n = 6). (H) Relative ROS level in lungs as assessed by DCF intensity (n = 6). (I) Inflammation score of Hematoxylin-Eosin staining (n = 6). (J) LDH activity in fresh lungs (n = 6). (K) Lung wet to dry ratio (n = 6). (L) Arterial blood gas analysis of PaO_2, $PaCO_2$ and TCO_2 (n = 6). Data are expressed as the mean ± SD. *$P <$ 0.05. NS indicates no significance.
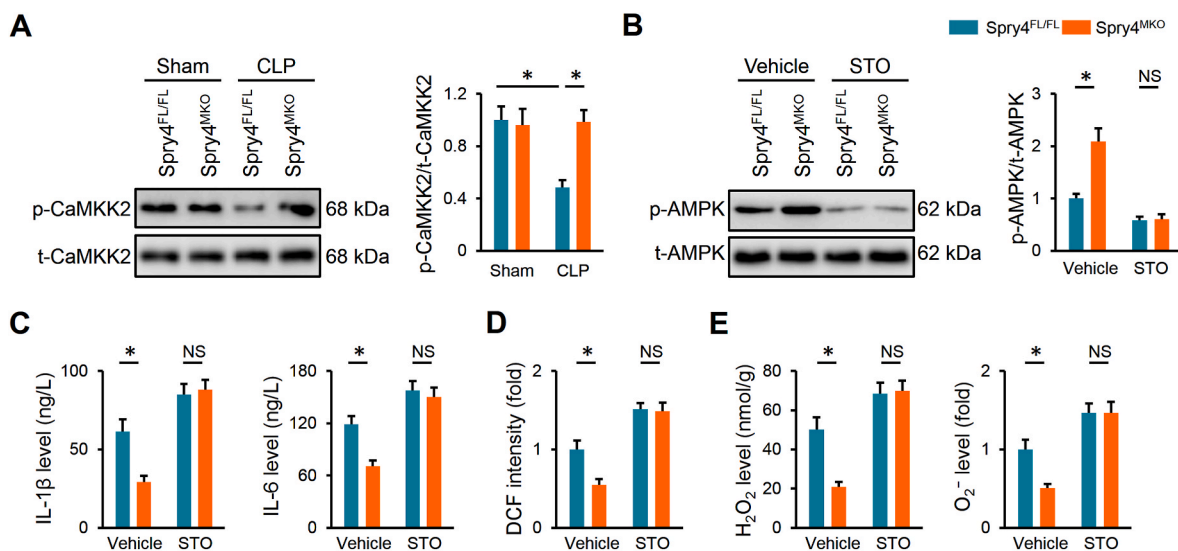
Fig. 7. Macrophage Spry4 deficiency activates AMPK pathway through CaMKK2. (A) Spry4$^{FL/FL}$ mice and Spry4^{MKO} mice were subjected to CLP surgery for 24 h, and CaMKK2 phosphorylation was detected using western blot (n = 6). (B) Spry4$^{FL/FL}$ or Spry4^{MKO} BMDMs were stimulated with LPS (100 ng/mL) for 12 h in the presence or absence of STO (5 mmol/L), and AMPK phosphorylation was detected using western blot (n = 6). (C) Quantification of IL-1β and IL-6 in cell medium (n = 6). (D) Relative ROS level in macrophages as assessed by DCF intensity (n = 6). (E) Quantification of H_2O_2 and O_2^- in macrophages (n = 6). Data are expressed as the mean ± SD. *$P < 0.05$. NS indicates no significance.

BMDMs after LPS stimulation (Fig. 7B). Accordingly, the inhibitory effects against LPS-induced inflammation and oxidative stress in Spry4^{MKO} BMDMs were also prevented by STO, as evidenced by increased IL-1β, IL-6, DCF intensity, H_2O_2 and O_2^- (Fig. 7C–E). Therefore, we prove that macrophage Spry4 deficiency activates AMPK pathway through CaMKK2.

4. Discussion

Our study for the first time documents the regulatory and predictive role of macrophage Spry4 in sepsis-induced inflammation, oxidative stress and ALI through controlling CaMKK2-dependent AMPK activation. Major findings are as follows: (i) macrophage Spry4 is increased in CLP mice and positively correlates with sepsis-induced ALI; (ii) macrophage Spry4 deficiency prevents sepsis-induced inflammation, oxidative stress and ALI in mice; (iii) macrophage Spry4 overexpression exacerbates sepsis-induced inflammation, oxidative stress and ALI in mice; (iv) Spry4 deficiency attenuates, while Spry4 overexpression promotes LPS-induced inflammation and oxidative stress in BMDMs; and (v) macrophage Spry4 deficiency alleviates sepsis-induced ALI through activating CaMKK2/AMPK pathway. Our study identify macrophage Spry4 as a promising predictive and therapeutic target of sepsis-induced ALI.

Excessive generations of inflammatory mediators and free radicals are implicated in the pathogenesis of sepsis-induced ALI. Upon sepsis, pathogen-associated molecular patterns and death-associated molecular patterns are released, and then activate Toll-like receptors to trigger phosphorylation and nuclear translocation of NF-κB, which subsequently induces the transcription of various inflammatory cytokines [39,40]. Of note, these cytokines, in turn, recruit and work on immune cells to further amplify sepsis-induced inflammation and cellular damage. Meanwhile, excessive accumulations of leukocytes also provoke overproductions of free radicals and then induce oxidative damage to biomacromolecules (e.g., lipid and protein). NRF2 is a central transcription factor to maintain redox homeostasis through triggering the expression of various anti-oxidant enzymes; however, its transcription activity in lungs is significantly suppressed during sepsis [15,41]. In line with previous studies, NF-κB was activated, while NRF2 was inactivated in CLP-injured lungs in our study, which were significantly prevented by macrophage Spry4 deficiency, accompanied by an improved inflammation and oxidative stress. Spry4 is implicated in the pathogenesis of

inflammatory diseases. Sharma et al. determined that Spry4 negatively regulated interferon signaling and associated biological processes that are implicated in the pathogenesis of sepsis-induced ALI [42]. And loss of Spry4 suppressed IL-1β receptor expression and subsequently ameliorated experimental autoimmune encephalomyelitis in mice [43]. Spry4 was also required for the migration and invasion of tumor cells, and macrophage Spry4 deficiency might inhibit the extravasation of circulation leukocytes. Increased vascular permeability, a key feature of sepsis-induced ALI, is essential for the leakage of fluid, proteins and circulating leukocytes, and contributes to the pulmonary inflammation, oxidative stress, edema and dysfunction during sepsis. Vascular endothelial growth factor A (VEGF-A) signaling plays critical roles in increasing vascular permeability; however Spry4 has been shown to negatively regulate VEGF-A pathway [44,45]. The protective effects of macrophage Spry4 deficiency against sepsis-induced ALI might be associated with the induction of VEGF-C pathway [46]. In addition, Spry4 silence facilitated the migration and adhesion of endothelial and epithelial cells that may also enhancing the reparative function of the lung during sepsis [47,48]. In line with our findings, results from Taniguchi et al. implied that Spry4 deficiency accelerated neovascularization and subsequently prevented ischemic injury of hind limb and soft tissue [49]. Meanwhile, Spry4 knockdown significantly enhanced neuronal survival and functional recovery [50]. The lung is composed of various cell types, and alveolar epithelial cells (AECs) are the main cell population in the lung. Various studies have shown that crosstalk between AECs and macrophages is essential to maintain lung homeostasis [51–53]. Mu et al. found that AECs-derived transforming growth factor-β acted on macrophages to suppress endogenous inflammatory signals during ALI [54]. Meanwhile, exosomes-derived from AECs significantly promoted the activation of macrophages, thereby exacerbating pulmonary inflammation of ALI mice [55]. In turn, macrophages, the major inflammatory cells in the lung, can also work on AECs and other cells to regulate lung homeostasis. Cakarova et al. found that TNF-α released from macrophages effectively regulated AECs proliferation and the restoration of alveolar barrier function [56]. And Ye et al. revealed that macrophages-derived exosomes and inflammatory cytokines activated neutrophils to amplify inflammation of ALI mice [57]. In this study, activities of NF-κB and NRF2, as well as expressions of downstream inflammatory cytokines and anti-oxidant enzymes were mainly analyzed in whole lung lysates in vivo. It is well-accepted that

both inflammatory cytokines and LPS can activate NF-κB, but inhibit NRF2 in AECs [58,59]. Whether the crosstalk between macrophage Spry4 regulated inflammation, oxidative stress and ALI through other cell populations (e.g., AECs or neutrophils) should be measured in further study.

AMPK, a pivotal regulator of intracellular energy homeostasis, has become a strategic target to treat sepsis-induced ALI. Increasing evidence indicate that AMPK activation can effectively suppress inflammation and oxidative stress, thereby preventing sepsis-induced ALI. Hu et al. recently reported that AMPK activation significantly suppress NF-κB phosphorylation and nuclear translocation, subsequently preventing aging-related inflammation in the myocardium [13]. Huang et al. previously demonstrated that AMPK activation could increase NRF2 expression in LPS-injured lungs and subsequently enhance the anti-oxidant capacity against LPS-induced ALI [8]. Receptor tyrosine kinases represent a large family intracellular signaling pathways, and are well-established regulators of various biological processes. Previous studies have shown that receptor tyrosine kinases signaling pathways and AMPK pathway influence reciprocally. Su et al. recently demonstrated that receptor tyrosine kinases MET controlled AMPK phosphorylation and activation in lung cancer [60]. And Xie et al. showed that targeting receptor tyrosine kinases EGFR could activate AMPK signaling pathway [61]. Spry4, a member of Spry proteins, is well-accepted as a kinase inhibitor, and previous studies have shown that Spry4 negatively regulates growth factors-induced receptor tyrosine kinases. Findings from Sasaki et al. revealed that Spry4 bound to Raf1 through the carboxy-terminal cysteine-rich domain, thereby inhibiting extracellular-signal-regulated kinase (ERK) pathway [44]. And Tian et al. reported that Spry4 silence activated ERK pathway, subsequently stimulated osteogenic differentiation and inhibited adipogenic differentiation of progenitor cells [62]. In the present study, we for the first time showed that macrophage Spry4 was a negative regulator of AMPK pathway, and macrophage Spry4 deficiency significantly activated AMPK during CLP-induced ALI. Moreover, we determined an involvement of CaMKK2 in macrophage Spry4 deficiency-mediated AMPK activation.

Despite we performed bone marrow transplantation and neutrophils deletion, and also constructed macrophage-specific Spry4 transgenic mice, whether macrophage-independent, myeloid-specific effects of Spry4 in Spry4^{MKO} mice remain further determination. Both Zhang et al. and Friedmacher et al. previously found that Spry4 in fetal lungs was mainly expressed in the epithelial tissue in mice and rats, especially in distal alveolar epithelium of newly formed airways [63,64]. Therefore, we speculated that epithelial Spry4 might also contribute to the progression of sepsis-induced ALI. However, the specific role and mechanism of Spry4 in other cell types should be well-determined in future studies. There are some additional limitations of the present study. First, the specific mechanisms mediating macrophage Spry4 upregulation were not investigated in this study. Second, whether other factors except inflammation and oxidative stress are involved in macrophage Spry4 deficiency-mediated pulmonoprotective effect need further investigation. Moreover, only male mice were used in this study, and the role and mechanism of macrophage Spry4 in female mice should also be discussed because of the effects of biological sex on sepsis treatments.

In summary, we reveal that macrophage Spry4 deficiency prevents sepsis-induced inflammation, oxidative stress and ALI in a CaMKK2/AMPK-dependent manner, and define it as a promising predictive and therapeutic target of sepsis-induced ALI.

Funding information

Author contributions

QTM, RC and CC designed the study. RC, CC, HML, WLJ and RP a collected the data. RC, CC, HH and KD analyzed and interpreted the work. RC and QTM drafted the manuscript. RC, CC and QTM revised it critically for important intellectual content. All authors contributed to the manuscript and approved the final version.

Supporting Information

Additional supporting information may be found online in the supporting Information section at the end of the article.

Declaration of competing interest

The authors declare that they have no known competing financial interests or personal relationships that could have appeared to influence the work reported in this paper.

Data availability

Data will be made available on request.

Appendix A. Supplementary data

Supplementary data related to this article can be found at https://doi.org/10.1016/j.redox.2022.102513.

References:

[1] T. van der Poll, M. Shankar-Hari, W.J. Wiersinga, The immunology of sepsis, Immunity 54 (11) (2021) 2450–2464.

[2] A. Poelzl, C. Lassnig, S. Tangermann, D. Hromadova, U. Reichart, R. Gawish, K. Mueller, R. Moriggl, A. Linkermann, M. Glosmann, L. Kenner, M. Mueller, B. Strobl, TYK2 licenses non-canonical inflammasome activation during endotoxemia, Cell Death Differ. 28 (2) (2021) 748–763.

[3] J. Shi, T. Yu, K. Song, S. Du, S. He, X. Hu, X. Li, H. Li, S. Dong, Y. Zhang, Z. Xie, C. Li, J. Yu, Dexmedetomidine ameliorates endotoxin-induced acute lung injury in vivo and in vitro by preserving mitochondrial dynamic equilibrium through the HIF-1a/HO-1 signaling pathway, Redox Biol. 41 (2021), 101954.

[4] Z. Feng, J. Zhou, Y. Liu, R. Xia, Q. Li, L. Yan, Q. Chen, X. Chen, Y. Jiang, G. Chao, M. Wang, G. Zhou, Y. Zhang, Y. Wang, H. Xia, Epithelium- and endothelium-derived exosomes regulate the alveolar macrophages by targeting RGS1 mediated calcium signaling-dependent immune response, Cell Death Differ. 28 (7) (2021) 2238–2256.

[5] H. Wang, X. Sun, Q. Lu, E.A. Zemskov, M. Yegambaram, X. Wu, T. Wang, H. Tang, S.M. Black, The mitochondrial redistribution of eNOS is involved in lipopolysaccharide induced inflammasome activation during acute lung injury, Redox Biol. 41 (2021) 101878.

[6] H.H. Yang, J.X. Duan, S.K. Liu, J.B. Xiong, X.X. Guan, W.J. Zhong, C.C. Sun, C.Y. Zhang, X.Q. Luo, Y.F. Zhang, P. Chen, B.D. Hammock, S.H. Hwang, J.X. Jiang, Y. Zhou, C.X. Guan, A COX-2/sEH dual inhibitor PTUPB alleviates lipopolysaccharide-induced acute lung injury in mice by inhibiting NLRP3 inflammasome activation, Theranostics 10 (11) (2020) 4749–4761.

[7] T. Wang, M. Yegambaram, C. Gross, X. Sun, Q. Lu, H. Wang, X. Wu, A. Kangath, H. Tang, S. Aggarwal, S.M. Black, RAC1 nitration at Y(32) IS involved in the endothelial barrier disruption associated with lipopolysaccharide-mediated acute lung injury, Redox Biol. 38 (2021) 101794.

[8] X.T. Huang, W. Liu, Y. Zhou, M. Sun, H.H. Yang, C.Y. Zhang, S.Y. Tang, Galectin-1 ameliorates lipopolysaccharide-induced acute lung injury via AMPK-Nrf2 pathway in mice, Free Radic. Biol. Med. 146 (2020) 222–233.

[9] K. Wang, Z. Zhang, H.I. Tsai, Y. Liu, J. Gao, M. Wang, L. Song, X. Cao, Z. Xu, H. Chen, A. Gong, D. Wang, F. Cheng, H. Zhu, Branched-chain amino acid aminotransferase 2 regulates ferroptotic cell death in cancer cells, Cell Death Differ. 28 (4) (2021) 1222–1236.

[10] X.S. Rao, X.X. Cong, X.K. Gao, Y.P. Shi, L.J. Shi, J.F. Wang, C.Y. Ni, M.J. He, Y. Xu, C. Yi, Z.X. Meng, J. Liu, P. Lin, L.L. Zheng, Y.T. Zhou, AMPK-mediated phosphorylation enhances the auto-inhibition of TBC1D17 to promote Rab5-dependent glucose uptake, Cell Death Differ. 28 (12) (2021) 3214–3234.

[11] S.Z. Fan, C.S. Lin, Y.W. Wei, S.R. Yeh, Y.H. Tsai, A.C. Lee, W.S. Lin, P.Y. Wang, Dietary citrate supplementation enhances longevity, metabolic health, and memory performance through promoting ketogenesis, Aging Cell 20 (12) (2021), e13510.

[12] H.J. Lee, A. Donati, D. Feliers, Y. Sun, Y. Ding, M. Madesh, A.B. Salmon, Y. Ikeno, C. Ross, C.L. O'Connor, W. Ju, M. Bitzer, Y. Chen, G.G. Choudhury, B.B. Singh, K. Sharma, B.S. Kasinath, Chloride channel accessory 1 integrates chloride channel

activity and mTORC1 in aging-related kidney injury, Aging Cell 20 (7) (2021), e13407.

[13] C. Hu, X. Zhang, M. Hu, T. Teng, Y.P. Yuan, P. Song, C.Y. Kong, S.C. Xu, Z.G. Ma, Q. Z. Tang, Fibronectin type III domain-containing 5 improves aging-related cardiac dysfunction in mice, Aging Cell 21 (3) (2022), e13556.

[14] Y. Yang, Z.T. Zhong, Y.G. Xiao, H.B. Chen, The activation of AMPK/NRF2 pathway in lung epithelial cells is involved in the protective effects of kinsenoside on lipopolysaccharide-induced acute lung injury, Oxid. Med. Cell. Longev. 2022 (2022), 3589277.

[15] W.L. Jiang, K.C. Zhao, W. Yuan, F. Zhou, H.Y. Song, G.L. Liu, J. Huang, J.J. Zou, B. Zhao, S.P. Xie, MicroRNA-31-5p exacerbates lipopolysaccharide-induced acute lung injury via inactivating Cab39/AMPKalpha pathway, Oxid. Med. Cell. Longev. 2020 (2020), 8822361.

[16] J.M. Mason, D.J. Morrison, M.A. Basson, J.D. Licht, Sprouty proteins: multifaceted negative-feedback regulators of receptor tyrosine kinase signaling, Trends Cell Biol. 16 (1) (2006) 45–54.

[17] W. Ding, S. Bellusci, W. Shi, D. Warburton, Genomic structure and promoter characterization of the human Sprouty4 gene, a novel regulator of lung morphogenesis, Am. J. Physiol. Lung Cell Mol. Physiol. 287 (1) (2004) L52–L59.

[18] K. Taniguchi, T. Ayada, K. Ichiyama, R. Kohno, Y. Yonemitsu, Y. Minami, A. Kikuchi, Y. Maehara, A. Yoshimura, Sprouty2 and Sprouty4 are essential for embryonic morphogenesis and regulation of FGF signaling, Biochem. Biophys. Res. Commun. 352 (4) (2007) 896–902.

[19] Y. Goldshmit, F. Frisca, J. Kaslin, A.R. Pinto, J.K. Tang, A. Pebay, R. Pinkas-Kramarski, P.D. Currie, Decreased anti-regenerative effects after spinal cord injury in spry4-/- mice, Neuroscience 287 (2015) 104–112.

[20] Y. Wang, D. Chen, H. Xie, M. Jia, X. Sun, F. Peng, F. Guo, D. Tang, AUF1 protects against ferroptosis to alleviate sepsis-induced acute lung injury by regulating NRF2 and ATF3, Cell. Mol. Life Sci. 79 (5) (2022) 228.

[21] X. Liu, J.W. Guo, X.C. Lin, Y.H. Tuo, W.L. Peng, S.Y. He, Z.Q. Li, Y.C. Ye, J. Yu, F. R. Zhang, M.M. Ma, J.Y. Shang, X.F. Lv, A.D. Zhou, Y. Ouyang, C. Wang, R.P. Pang, J.X. Sun, J.S. Ou, J.G. Zhou, S.J. Liang, Macrophage NFATc3 prevents foam cell formation and atherosclerosis: evidence and mechanisms, Eur. Heart J. 42 (47) (2021) 4847–4861.

[22] J. Rao, J. Qiu, M. Ni, H. Wang, P. Wang, L. Zhang, Z. Wang, M. Liu, F. Cheng, X. Wang, L. Lu, Macrophage nuclear factor erythroid 2-related factor 2 deficiency promotes innate immune activation by tissue inhibitor of metalloproteinase 3-mediated RhoA/ROCK pathway in the ischemic liver, Hepatology 75 (6) (2022) 1429–1445.

[23] S. Manzoor, N. Mariappan, I. Zafar, C.C. Wei, A. Ahmad, R. Surolia, J.B. Foote, A. Agarwal, S. Ahmad, M. Athar, V.B. Antony, A. Ahmad, Cutaneous lewisite exposure causes acute lung injury, Ann. N. Y. Acad. Sci. 1479 (1) (2020) 210–222.

[24] S. Rayees, J.C. Joshi, M. Tauseef, M. Anwar, S. Baweja, I. Rochford, B. Joshi, M. D. Hollenberg, S.P. Reddy, D. Mehta, PAR2-Mediated cAMP generation suppresses TRPV4-dependent Ca(2+) signaling in alveolar macrophages to resolve TLR4-induced inflammation, Cell Rep. 27 (3) (2019) 793–805.

[25] X. Xu, G. Ding, C. Liu, Y. Ding, X. Chen, X. Huang, C.S. Zhang, S. Lu, Y. Zhang, Y. Huang, Z. Chen, W. Wei, L. Liao, S.H. Lin, J. Li, W. Liu, J. Li, S.C. Lin, X. Ma, J. Wong, Nuclear UHRF1 is a gate-keeper of cellular AMPK activity and function, Cell Res. 32 (1) (2022) 54–71.

[26] X. Zhang, J.X. Zhu, Z.G. Ma, H.M. Wu, S.C. Xu, P. Song, C.Y. Kong, Y.P. Yuan, W. Deng, Q.Z. Tang, Rosmarinic acid alleviates cardiomyocyte apoptosis via cardiac fibroblast in doxorubicin-induced cardiotoxicity, Int. J. Biol. Sci. 15 (3) (2019) 556–567.

[27] Y. Hou, Q. Zhang, W. Pang, L. Hou, Y. Liang, X. Han, X. Luo, P. Wang, X. Zhang, L. Li, X. Meng, YTHDC1-mediated augmentation of miR-30d in repressing pancreatic tumorigenesis via attenuation of RUNX1-induced transcriptional activation of Warburg effect, Cell Death Differ. 28 (11) (2021) 3105–3124.

[28] X. Zhang, Z.G. Ma, Y.P. Yuan, S.C. Xu, W.Y. Wei, P. Song, C.Y. Kong, W. Deng, Q. Z. Tang, Rosmarinic acid attenuates cardiac fibrosis following long-term pressure overload via AMPKalpha/Smad3 signaling, Cell Death Dis. 9 (2) (2018) 102.

[29] Y. Liu, B.A. Bell, Y. Song, H.J. Kim, J.K. Sterling, B.J. Kim, M. Poli, M. Guo, K. Zhang, A. Rao, J.R. Sparrow, G. Su, J.L. Dunaief, Intraocular iron injection induces oxidative stress followed by elements of geographic atrophy and sympathetic ophthalmia, Aging Cell 20 (11) (2021), e13490.

[30] X. Zhang, C. Hu, N. Zhang, W.Y. Wei, L.L. Li, H.M. Wu, Z.G. Ma, Q.Z. Tang, Matrine attenuates pathological cardiac fibrosis via RPS5/p38 in mice, Acta Pharmacol. Sin. 42 (4) (2021) 573–584.

[31] X. Zhang, C. Hu, Y.P. Yuan, P. Song, C.Y. Kong, H.M. Wu, S.C. Xu, Z.G. Ma, Q. Z. Tang, Endothelial ERG alleviates cardiac fibrosis via blocking endothelin-1-dependent paracrine mechanism, Cell Biol. Toxicol. 37 (6) (2021) 873–890.

[32] J. Sun, T. Jin, W. Su, Y. Guo, Z. Niu, J. Guo, L. Li, J. Wang, L. Ma, T. Yu, X. Li, Y. Zhou, H. Shan, H. Liang, The long non-coding RNA PFI protects against pulmonary fibrosis by interacting with splicing regulator SRSF1, Cell Death Differ. 28 (10) (2021) 2916–2930.

[33] X. Zhang, C. Hu, X.P. Yuan, Y.P. Yuan, P. Song, C.Y. Kong, T. Teng, M. Hu, S.C. Xu, Z.G. Ma, Q.Z. Tang, Osteocrin, a novel myokine, prevents diabetic cardiomyopathy via restoring proteasomal activity, Cell Death Dis. 12 (7) (2021) 624.

[34] C. Hu, X. Zhang, P. Song, Y.P. Yuan, C.Y. Kong, H.M. Wu, S.C. Xu, Z.G. Ma, Q. Z. Tang, Meteorin-like protein attenuates doxorubicin-induced cardiotoxicity via activating cAMP/PKA/SIRT1 pathway, Redox Biol. 37 (2020), 101747.

[35] X. Zhang, C. Hu, Y.C. Kong, P. Song, H.M. Wu, S.C. Xu, Y.P. Yuan, W. Deng, Z. G. Ma, Q.Z. Tang, FNDC5 alleviates oxidative stress and cardiomyocyte apoptosis in doxorubicin-induced cardiotoxicity via activating AKT, Cell Death Differ. 27 (2) (2020) 540–555.

[36] S. Matsushima, J. Kuroda, T. Ago, P. Zhai, Y. Ikeda, S. Oka, G.H. Fong, R. Tian, J. Sadoshima, Broad suppression of NADPH oxidase activity exacerbates ischemia/reperfusion injury through inadvertent downregulation of hypoxia-inducible factor-1alpha and upregulation of peroxisome proliferator-activated receptor-alpha, Circ. Res. 112 (8) (2013) 1135–1149.

[37] C. Hu, X. Zhang, W. Wei, N. Zhang, H. Wu, Z. Ma, L. Li, W. Deng, Q. Tang, Matrine attenuates oxidative stress and cardiomyocyte apoptosis in doxorubicin-induced cardiotoxicity via maintaining AMPKalpha/UCP2 pathway, Acta Pharm. Sin. B 9 (4) (2019) 690–701.

[38] C. Hu, X. Zhang, N. Zhang, W.Y. Wei, L.L. Li, Z.G. Ma, Q.Z. Tang, Osteocrin attenuates inflammation, oxidative stress, apoptosis, and cardiac dysfunction in doxorubicin-induced cardiotoxicity, Clin. Transl. Med. 10 (3) (2020) e124.

[39] M. Haselager, R. Thijssen, C. West, L. Young, R. Van Kampen, E. Willmore, S. Mackay, A. Kater, E. Eldering, Regulation of Bcl-XL by non-canonical NF-kappaB in the context of CD40-induced drug resistance in CLL, Cell Death Differ. 28 (5) (2021) 1658–1668.

[40] J.A. Fafian-Labora, A. O'Loghlen, NF-kappaB/IKK activation by small extracellular vesicles within the SASP, Aging Cell 20 (7) (2021), e13426.

[41] Y. Li, Y.F. Feng, X.T. Liu, Y.C. Li, H.M. Zhu, M.R. Sun, P. Li, B. Liu, H. Yang, Songorine promotes cardiac mitochondrial biogenesis via Nrf2 induction during sepsis, Redox Biol. 38 (2021), 101771.

[42] B. Sharma, S. Joshi, A. Sassano, B. Majchrzak, S. Kaur, P. Aggarwal, B. Nabet, M. Bulic, B.L. Stein, B. McMahon, D.P. Baker, R. Fukunaga, J.K. Altman, J.D. Licht, E.N. Fish, L.C. Platanias, Sprouty proteins are negative regulators of interferon (IFN) signaling and IFN-inducible biological responses, J. Biol. Chem. 287 (50) (2012) 42352–42360.

[43] T. Fukaya, K. Someya, S. Hibino, M. Okada, H. Yamane, K. Taniguchi, A. Yoshimura, Loss of Sprouty4 in T cells ameliorates experimental autoimmune encephalomyelitis in mice by negatively regulating IL-1beta receptor expression, Biochem. Biophys. Res. Commun. 447 (3) (2014) 471–478.

[44] A. Sasaki, T. Taketomi, R. Kato, K. Saeki, A. Nonami, M. Sasaki, M. Kuriyama, N. Saito, M. Shibuya, A. Yoshimura, Mammalian Sprouty4 suppresses ras-independent ERK activation by binding to Raf1, Nat. Cell Biol. 5 (5) (2003) 427–432.

[45] T. Ayada, K. Taniguchi, F. Okamoto, R. Kato, S. Komune, G. Takaesu, A. Yoshimura, Sprouty4 negatively regulates protein kinase C activation by inhibiting phosphatidylinositol 4,5-biphosphate hydrolysis, Oncogene 28 (8) (2009) 1076–1088.

[46] M. Yamashita, M. Niisato, Y. Kawasaki, S. Karaman, M.R. Robciuc, Y. Shibata, Y. Ishida, R. Nishio, T. Masuda, T. Sugai, M. Ono, R.M. Tuder, K. Alitalo, K. Yamauchi, VEGF-C/VEGFR-3 signalling in macrophages ameliorates acute lung injury, Eur. Respir. J. 59 (4) (2022).

[47] Y. Gong, X. Yang, Q. He, L. Gower, I. Prudovsky, C.P. Vary, P.C. Brooks, R. E. Friesel, Sprouty4 regulates endothelial cell migration via modulating integrin beta3 stability through c-Src, Angiogenesis 16 (4) (2013) 861–875.

[48] J. Shi, X. Ma, Y. Su, Y. Song, Y. Tian, S. Yuan, X. Zhang, D. Yang, H. Zhang, J. Shuai, W. Cui, F. Ren, M.V. Plikus, Y. Chen, J. Luo, Z. Yu, MiR-31 mediates inflammatory signaling to promote Re-epithelialization during skin wound healing, J. Invest. Dermatol. 138 (10) (2018) 2253–2263.

[49] K. Taniguchi, K. Sasaki, K. Watari, H. Yasukawa, T. Imaizumi, T. Ayada, F. Okamoto, T. Ishizaki, R. Kato, R. Kohno, H. Kimura, Y. Sato, M. Ono, Y. Yonemitsu, A. Yoshimura, Suppression of Sproutys has a therapeutic effect for a mouse model of ischemia by enhancing angiogenesis, PLoS One 4 (5) (2009) e5467.

[50] L. Klimaschewski, B.P. Sueiro, L.M. Millan, siRNA mediated down-regulation of Sprouty2/4 diminishes ischemic brain injury, Neurosci. Lett. 612 (2016) 48–51.

[51] E.Y. Bissonnette, J.F. Lauzon-Joset, J.S. Debley, S.F. Ziegler, Cross-talk between alveolar macrophages and lung epithelial cells is essential to maintain lung homeostasis, Front. Immunol. 11 (2020), 583042.

[52] J. Gschwend, S. Sherman, F. Ridder, X. Feng, H.E. Liang, R.M. Locksley, B. Becher, C. Schneider, Alveolar macrophages rely on GM-CSF from alveolar epithelial type 2 cells before and after birth, J. Exp. Med. (10) (2021) 218.

[53] C.L. Scott, M. Guilliams, Tissue unit-ed: lung cells team up to drive alveolar macrophage development, Cell 175 (4) (2018) 898–900.

[54] M. Mu, P. Gao, Q. Yang, J. He, F. Wu, X. Han, S. Guo, Z. Qian, C. Song, Alveolar epithelial cells promote IGF-1 production by alveolar macrophages through TGF-beta to suppress endogenous inflammatory signals, Front. Immunol. 11 (2020) 1585.

[55] F. Liu, W. Peng, J. Chen, Z. Xu, R. Jiang, Q. Shao, N. Zhao, K. Qian, Exosomes derived from alveolar epithelial cells promote alveolar macrophage activation mediated by miR-92a-3p in sepsis-induced acute lung injury, Front. Cell. Infect. Microbiol. 11 (2021), 646546.

[56] L. Cakarova, L.M. Marsh, J. Wilhelm, K. Mayer, F. Grimminger, W. Seeger, J. Lohmeyer, S. Herold, Macrophage tumor necrosis factor-alpha induces epithelial expression of granulocyte-macrophage colony-stimulating factor: impact on alveolar epithelial repair, Am. J. Respir. Crit. Care Med. 180 (6) (2009) 521–532.

[57] C. Ye, H. Li, M. Bao, R. Zhuo, G. Jiang, W. Wang, Alveolar macrophage - derived exosomes modulate severity and outcome of acute lung injury, Aging (Albany NY) 12 (7) (2020) 6120–6128.

[58] C.C. Yang, L.D. Hsiao, C.Y. Wang, W.N. Lin, Y.F. Shih, Y.W. Chen, R.L. Cho, H. C. Tseng, C.M. Yang, HO-1 upregulation by kaempferol via ROS-dependent Nrf2-ARE cascade attenuates lipopolysaccharide-mediated intercellular cell adhesion molecule-1 expression in human pulmonary alveolar epithelial cells, Antioxidants 11 (4) (2022).

[59] Z. Fu, Z. Jiang, G. Guo, X. Liao, M. Liu, Z. Xiong, rhKGF-2 attenuates smoke inhalation lung injury of rats via activating PI3K/Akt/Nrf2 and repressing FoxO1-NLRP3 inflammasome, Front. Pharmacol. 12 (2021), 641308.

[60] LINC00857 W. Su, L. Wang, H. Zhao, S. Hu, Y. Zhou, C. Guo, B. Wu, L. Li, Z. Yang, D.G. Beer, G. Chen, Interacting with YBX1 to regulate apoptosis and autophagy via MET and phosphor-AMPKa signaling, Mol. Ther. Nucleic Acids 22 (2020) 1164–1175.

[61] Y.J. Xie, W.N. Gao, Q.B. Wu, X.J. Yao, Z.B. Jiang, Y.W. Wang, W.J. Wang, W. Li, S. Hussain, L. Liu, E.L. Leung, X.X. Fan, Chelidonine selectively inhibits the growth of gefitinib-resistant non-small cell lung cancer cells through the EGFR-AMPK pathway, Pharmacol. Res. 159 (2020), 104934.

[62] L. Tian, H. Xiao, M. Li, X. Wu, Y. Xie, J. Zhou, X. Zhang, B. Wang, A novel Sprouty4-ERK1/2-Wnt/beta-catenin regulatory loop in marrow stromal progenitor cells controls osteogenic and adipogenic differentiation, Metabolism 105 (2020), 154189.

[63] S. Zhang, Y. Lin, P. Itaranta, A. Yagi, S. Vainio, Expression of Sprouty genes 1, 2 and 4 during mouse organogenesis, Mech. Dev. 109 (2) (2001) 367–370.

[64] F. Friedmacher, J.H. Gosemann, N. Fujiwara, H. Takahashi, A. Hofmann, P. Puri, Expression of Sproutys and SPREDs is decreased during lung branching morphogenesis in nitrofen-induced pulmonary hypoplasia, Pediatr. Surg. Int. 29 (11) (2013) 1193–1198.